Enhancing the sensitivity of nonlinearity sensors through homodyne detection in dissipatively coupled systems

Dianzhen Cui,[1] Jianning Li,[1] Fude Li,[1] Zhi-Cheng Shi,[3,4] and X. X. Yi[1,2,*]

[1]*Center for Quantum Sciences and School of Physics, Northeast Normal University, Changchun 130024, China*
[2]*Center for Advanced Optoelectronic Functional Materials Research and Key Laboratory for UV Light-Emitting Materials and Technology of Ministry of Education, Northeast Normal University, Changchun 130024, China*
[3]*Fujian Key Laboratory of Quantum Information and Quantum Optics, Fuzhou University, Fuzhou 350108, China*
[4]*Department of Physics, Fuzhou University, Fuzhou 350108, China*

(Received 20 July 2022; revised 15 November 2022; accepted 5 January 2023; published 17 January 2023)

In this paper, we propose a sensing mechanism to enhance the sensitivity of a quantum system to nonlinearities by homodyning the amplitude quadrature of the cavity field. The system consists of two dissipatively coupled cavity modes, one of which is subject to single- and two-photon drives. In the regime of low two-photon driving strength, the spectrum of the system acquires a real spectral singularity. We find that this singularity is very sensitive to the two-photon drive and nonlinearity of the system, and compared to the previous nonlinearity sensor, the proposed sensor achieves an unprecedented sensitivity around the singularity point. Moreover, the scheme is robust against fabrication imperfections. This work would open a different avenue for quantum sensors, which could find applications in many fields, such as precise measurement and quantum metrology.

DOI: 10.1103/PhysRevA.107.013709

I. INTRODUCTION

Hermiticity and real eigenvalues of the Hamiltonian in closed systems are the key postulate in quantum mechanics. In recent years, it was discovered that the axiom of Hermiticity can be replaced by the condition of parity-time ($\mathcal{PT}$) symmetry, leading to the foundations of non-Hermitian quantum mechanics [1,2]. Interestingly, non-Hermitian Hamiltonians also exhibit entirely real eigenvalues when satisfying $[H, \mathcal{PT}] = 0$, where $\mathcal{PT}$ is the joint parity-time operator. A more significant feature of such Hamiltonians is the breaking of the $\mathcal{PT}$ symmetry, in which the eigenspectrum switches from purely real to completely imaginary [3–25]. This sudden $\mathcal{PT}$ phase transition is marked by the exceptional point (EP), associated with level coalescence, in which the eigenvalues and their corresponding eigenvectors simultaneously coalesce and become degenerate. Recently, the $\mathcal{PT}$ phase transition was experimentally observed in various $\mathcal{PT}$-symmetric systems [26–29].

As a counterpart, the anti-parity-time symmetry, where the Hamiltonian of the system is anticommutative with the joint $\mathcal{PT}$ operator (mathematically, $\{H, \mathcal{PT}\} = 0$), has recently attracted great interest [30–46]. In contrast to the $\mathcal{PT}$-symmetric system, the anti-$\mathcal{PT}$-symmetric system does not require gain, but it can still exhibit an EP with purely imaginary eigenvalues. This characteristic is of great significance for realizing non-Hermitian dynamics in the quantum domain without Langevin noise [47]. To date, several relevant experiments have been realized in different physical systems, including cold atoms [37], optics [43], magnon-cavity hybrid systems [39], electrical circuit resonators [40], and integrated photonics [41,42].

Sensitivity enhancement based on EPs has been demonstrated both theoretically and experimentally [17–21,45–55] in particle detectors [17], mass sensors [51], and gyroscopes [54]. It has been shown that if an EP is subjected to the strength ϵ of the *linear* perturbation, the frequency splitting (the energy spacing of the two levels) scales as the square root of the perturbation strength ϵ [17–21,45–55]. Recently, in the context of dissipatively coupled anti-$\mathcal{PT}$-symmetric systems, a scheme was proposed to efficiently detect the *nonlinear* perturbations [31]. This dissipatively coupled system has an imaginary coupling strength [31], resulting from the fact that the vacuum of the electromagnetic field can produce coherence in the process of spontaneous emission [56]. Owing to this coherence, the system acquires a real spectral singularity which strongly suppresses the linewidth of a resonance spectrum, thereby drawing out a remarkable response. Particularly, near the coherence-induced singularity (CIS), the response $\mathcal{N}$ behaves as $|\frac{d\mathcal{N}}{dU}| \propto |U|^{-5/3}$, where U quantifies the strength of the Kerr nonlinearity [31]. Compared with EP-based sensors [17–21,45–55], the sensitivity of the system to inherent nonlinearities has been greatly improved, and the protocol does not require any gains [31].

To enhance the sensitivity of quantum sensors, in this paper, we theoretically propose a sensing mechanism to improve the sensitivity of a quantum system to nonlinearities. Our proposal is based on two dissipatively coupled cavity modes, one of which is subject to single- and two-photon drives. The key point of our sensing protocol is that the spectrum of the dissipatively coupled system acquires a CIS at the low two-photon driving strength. In the vicinity of the CIS, the current sensing protocol exhibits a much larger sensitivity compared with the

*yixx@nenu.edu.cn

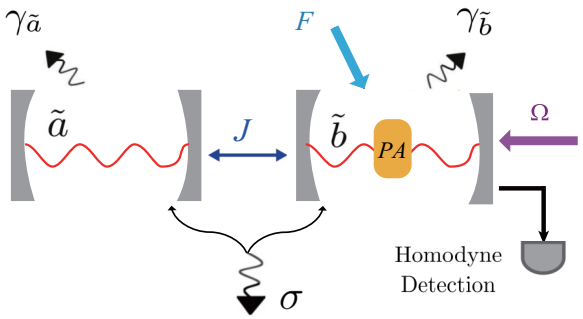

FIG. 1. Illustration of our setup. The cavity modes $\tilde{a}$ and $\tilde{b}$ are dissipatively coupled through the shared dissipative environment. $\gamma_{\tilde{a}}$ and $\gamma_{\tilde{b}}$ denote the dissipation rates of systems $\tilde{a}$ and $\tilde{b}$, respectively. σ stands for the cooperative interactions between the two modes and the common reservoir. J is the direct coupling between the cavity modes. The cavity mode $\tilde{b}$ is driven by a single-photon pump of amplitude Ω. The cavity mode $\tilde{b}$ is also subject to a classical pump of amplitude F. A parametric amplifier (PA) is inserted inside the cavity $\tilde{b}$. By using a homodyne setup, the nonlinear parameter is estimated via the amplitude quadrature of the cavity field $\tilde{b}$. See the text for details.

previous work [31]. The proposed sensor differs from known sensors in at least five points: (i) it operates at a CIS instead of the EP, (ii) it can help to estimate two types of nonlinear parameters (Kerr nonlinearity coefficient and two-photon driving amplitude), (iii) the nonlinear parameters are estimated via the amplitude quadrature of the cavity field and can reach an unprecedented sensitivity around the CIS, (iv) we need to increase the two-photon driving amplitude only slightly to overcome the deleterious effects of fabrication imperfections, and (v) it works without the requirement of anti-$\mathcal{PT}$ symmetry, making such a configuration much more accessible.

The remainder of this paper is organized as follows. In Sec. II, a physical model is introduced to describe the setup, and the dynamical equations for the system are derived. In Sec. III, we study the sensitivity of the system to nonlinearities and discuss the effect of the fabrication imperfections on the performance of the setup. In Sec. IV, we discuss the experimental feasibility of the present scheme. Finally, the conclusions are drawn in Sec. V. In the Appendix, we discuss the validity of the mean-field approximation.

II. MODEL AND DYNAMICAL EQUATIONS

The schematic diagram is sketched in Fig. 1. We consider a general situation where we have two dissipatively coupled cavity modes, one of which is subject to single- and two-photon drives. In the rotating frame with respect to frequency ω_p of the laser, the total Hamiltonian of the system reads ($\hbar = 1$) [31,57]

$$H = H_f + H_k + H_i + H_l + H_s, \tag{1}$$

with

$$\begin{aligned} H_f &= \Delta_{\tilde{a}} a^\dagger a + \Delta_{\tilde{b}} b^\dagger b, \quad H_k = U(b^{\dagger 2} b^2), \\ H_i &= J(ab^\dagger + a^\dagger b), \quad H_l = \Omega(b^\dagger + b), \\ H_s &= G(e^{-i\theta_p} b^{\dagger 2} + e^{i\theta_p} b^2). \end{aligned} \tag{2}$$

Here, H_f represents the free Hamiltonian of the uncoupled cavity modes $\tilde{a}$ and $\tilde{b}$, and $a^\dagger$ ($b^\dagger$) and a (b) are the creation and annihilation operators of mode $\tilde{a}$ ($\tilde{b}$), respectively. $\Delta_j = \omega_j - \omega_p/2$ ($j = \tilde{a}, \tilde{b}$) represents the detuning of modes $\tilde{a}$ and $\tilde{b}$ with respect to the laser field, and the frequencies of modes $\tilde{a}$ and $\tilde{b}$ are $\omega_{\tilde{a}}$ and $\omega_{\tilde{b}}$, respectively. The Hamiltonian H_k describes the Kerr nonlinearity of mode $\tilde{b}$, and the strength is denoted by U [58–63]. The Hamiltonian H_i describes the direct coupling between the modes with coupling strength J. The Hamiltonian H_l represents mode $\tilde{b}$ driven coherently by a single-photon pump with amplitude Ω and frequency $\omega_l = \omega_p/2$. The Hamiltonian H_s describes mode $\tilde{b}$ subjected to a two-photon drive of amplitude G, frequency ω_p, and phase θ_p. We will demonstrate later how to adjust θ_p to enhance the response of the system to Kerr nonlinearity. Physically, a squeezed laser can be obtained by means of the degenerate parametric down-converter [64]. A certain kind of nonlinear medium is pumped by a field of frequency ω_p, and the photons of that field are converted into pairs of identical photons, of frequency $\omega_p/2$ each, into the signal field. This process is known as the degenerate parametric down-conversion, and it can be implemented in a system described by the Hamiltonian

$$\begin{aligned} H =& \omega_{\tilde{a}} a^\dagger a + \omega_{\tilde{b}} b^\dagger b + J(ab^\dagger + a^\dagger b) + U b^\dagger b^\dagger bb \\ &+ \Omega(b^\dagger e^{-i\omega_l t} + be^{i\omega_l t}) + \omega_p c^\dagger c + \chi^{(2)}(b^2 c^\dagger + b^{\dagger 2} c), \end{aligned}$$

where ω_p is the frequency of the pump mode and $\chi^{(2)}$ is a second-order nonlinear susceptibility [65]. We now assume that the pump field is classical, such that its photons remains undepleted over the relevant timescale. Suppose that the field is in coherent state $|\Lambda e^{-i\omega_p t}\rangle$ ($\Lambda = Fe^{-i\theta_p}$), and approximate operators c and $c^\dagger$ by $\Lambda e^{-i\omega_p t}$ and $\Lambda^* e^{i\omega_p t}$, respectively; the above Hamiltonian reduces to

$$\begin{aligned} H =& \omega_{\tilde{a}} a^\dagger a + \omega_{\tilde{b}} b^\dagger b + J(ab^\dagger + a^\dagger b) + U b^\dagger b^\dagger bb \\ &+ \Omega(b^\dagger e^{-i\omega_l t} + be^{i\omega_l t}) + (\tilde{G}^* b^2 e^{i\omega_p t} + \tilde{G} b^{\dagger 2} e^{-i\omega_p t}), \end{aligned}$$

where $\tilde{G} = \chi^{(2)}\Lambda = Ge^{-i\theta_p}$. In the rotating frame defined by $U = \exp[(-i\frac{\omega_p}{2} a^\dagger a - i\frac{\omega_p}{2} b^\dagger b)t]$, the above Hamiltonian becomes

$$\begin{aligned} H =& \Delta_{\tilde{a}} a^\dagger a + \Delta_{\tilde{b}} b^\dagger b + J(ab^\dagger + a^\dagger b) + U b^\dagger b^\dagger bb \\ &+ \Omega(b^\dagger e^{-i\Delta_l t} + be^{i\Delta_l t}) + (\tilde{G}^* b^2 + \tilde{G} b^{\dagger 2}), \end{aligned}$$

where $\Delta_{\tilde{a}/\tilde{b}} = \omega_{\tilde{a}/\tilde{b}} - \omega_p/2$ and $\Delta_l = \omega_l - \omega_p/2$. Recently, this two-photon drive was realized by coupling two superconducting resonators through a Josephson junction [66]. On the other hand, the dissipative environment can be roughly divided into two categories: one in which the modes are coupled independently to their local reservoirs and one in which a common reservoir interacts with both, as shown in Fig. 1.

A complete description of the two-mode system interacting with the dissipative environment is the master equation in the Lindblad form [56,67],

$$\frac{d\rho}{dt} = -i[H, \rho] + \gamma_{\tilde{a}} \mathcal{L}[a]\rho + \gamma_{\tilde{b}} \mathcal{L}[b]\rho + \sigma \mathcal{L}[c]\rho, \tag{3}$$

where the second and third terms represent the intrinsic damping of modes $\tilde{a}$ and $\tilde{b}$, respectively. The fourth term describes the cooperative interactions between the two modes and the common reservoir. The standard dissipative superoperator

$\mathcal{L}[o]$ is defined by $\mathcal{L}[o]\rho = 2o\rho o^\dagger - o^\dagger o\rho - \rho o^\dagger o$, and the jump operator c is a linear superposition of the annihilation operators a and b, $c \to \nu a + u e^{i\theta} b$. If the phase difference θ of light propagation from one mode to another is a multiple of 2π, the jump operator has the general form $c \to \nu a + ub$ [67], where the coefficients ν and u represent the couplings of the two modes to the common reservoir, respectively. If the two modes are symmetrically coupled to the common reservoir, the operator c is expressed as $c = (1/\sqrt{2})(a + b)$. The external damping rates induced by the common reservoir for the two modes are $\sigma\nu^2 = \kappa_{\tilde{a}}$ and $\sigma u^2 = \kappa_{\tilde{b}}$, respectively. The cooperative dissipations between the two modes is $\sigma\nu u = \sqrt{\kappa_{\tilde{a}}\kappa_{\tilde{b}}}$, where the $\sqrt{\kappa_{\tilde{a}}\kappa_{\tilde{b}}}$ represents the effect of quantum interference resulting from the cross coupling between the two modes. Without loss of generality, we assume that the parameters γ_j and κ_j $(j = \tilde{a}, \tilde{b})$ are the same for the whole system, i.e., $\gamma_{\tilde{a}} = \gamma_{\tilde{b}} = \gamma_0$ and $\kappa_{\tilde{a}} = \kappa_{\tilde{b}} = \Gamma$.

III. SENSITIVITY AT THE COHERENCE-INDUCED SINGULARITY

A. Effective Hamiltonian and the sensitivity of the system to nonlinearities

Starting from the Lindblad master equation in Eq. (3), we can obtain the mean-value equations for modes $\tilde{a}$ and $\tilde{b}$ via the relation $\langle\dot{\zeta}\rangle = \mathrm{Tr}(\dot{\rho}\zeta)$ [56]:

$$\begin{aligned}
\dot{\alpha} =& -i[\Delta_{\tilde{a}} - i(\gamma_0 + \Gamma)]\alpha - i(J - i\Gamma)\beta,\\
\dot{\beta} =& -i(J - i\Gamma)\alpha - i[\Delta_{\tilde{b}} - i(\gamma_0 + \Gamma)]\beta\\
&- 2iU|\beta|^2\beta - 2iG\beta^* - i\Omega,\\
\dot{\alpha^*} =& (\dot{\alpha})^*,\\
\dot{\beta^*} =& (\dot{\beta})^*,
\end{aligned} \tag{4}$$

where $\dot{\alpha} = \langle\dot{a}\rangle$, $\dot{\beta} = \langle\dot{b}\rangle$, and we set $\theta_p = 0$. In the derivation of Eq. (4), we have adopted the mean-field approximation, i.e., $\langle b^\dagger bb\rangle \approx \langle b^\dagger\rangle\langle b\rangle\langle b\rangle$. In the next sections, we work in the parameter interval, in which the mean-field approximation is a good approximation (more details are given in the Appendix). It is obvious to observe from the above expressions that the effective dissipative coupling strength between the two modes is $i\Gamma$, which originates from the bath-mediated collective damping.

To study the performance of the proposed sensor, we need to solve the eigenvalues of the effective optical system and find the CIS feature. The equivalent Schrödinger-like equation in this configuration obeys $i\frac{d\phi}{dt} = H_{\mathrm{eff}}\phi$, where $\phi = (\alpha, \beta, \alpha^*, \beta^*)^T$ is the state vector, and the form of the associated effective Hamiltonian H_{eff} is

$$H_{\mathrm{eff}} = \begin{pmatrix}
\Delta_{\tilde{a}} - i(\gamma_0 + \Gamma) & J - i\Gamma & 0 & 0\\
J - i\Gamma & \Delta_{\tilde{b}} - i(\gamma_0 + \Gamma) + 2\tilde{U} & 0 & 2G\\
0 & 0 & -\Delta_{\tilde{a}} - i(\gamma_0 + \Gamma) & -J - i\Gamma\\
0 & -2G & -J - i\Gamma & -\Delta_{\tilde{b}} - i(\gamma_0 + \Gamma) - 2\tilde{U}
\end{pmatrix}, \tag{5}$$

where $\tilde{U} = U|\beta|^2$. Notably, the effective Hamiltonian (5) does not have the anti-$\mathcal{PT}$ symmetry. Therefore, our system is easier to obtain than previous schemes [31,45]. The effective Hamiltonian H_{eff} has four eigenvalues forming two pairs, and one pair is due to the appearance of α^* and β^* in the dynamics.

In the limit of the weak two-photon driving amplitude G, we can bring the effective Hamiltonian into a block-diagonal form, and we will study the block corresponding to α and β in the following:

$$\tilde{H}_{\mathrm{eff}} = \begin{pmatrix}
\Delta_{\tilde{a}} - i(\gamma_0 + \Gamma) & J - i\Gamma\\
J - i\Gamma & \tilde{\Delta}_{\tilde{b}} - i(\gamma_0 + \Gamma)
\end{pmatrix}, \tag{6}$$

where $\tilde{\Delta}_{\tilde{b}} = \Delta_{\tilde{b}} + 2\tilde{U}$. Without loss of generality, we choose the parameter as follows: $\Delta_{\tilde{a}} = -\Delta_{\tilde{b}} = \delta/2$, $J = 0$, and $\tilde{U} = 10^{-3}\ \Gamma$, which are similar to the parameters chosen in Ref. [31]. The eigenvalues of Eq. (6) are given by

$$\begin{aligned}
\tilde{\lambda}_\pm &= \tilde{U} - i(\gamma_0 + \Gamma) \pm \frac{1}{2}\sqrt{4\tilde{U}^2 - 4\Gamma^2 - 4\tilde{U}\delta + \delta^2}\\
&\approx -i(\gamma_0 + \Gamma) \pm \sqrt{\frac{\delta^2}{4} - \Gamma^2}.
\end{aligned} \tag{7}$$

With the intrinsic damping γ_0 of the mode approaching zero, one of the eigenvalues characterizing its dynamics tends to the real axis at $\delta = 0$. The dissipative coupling strength $i\Gamma$ can be viewed as an effective gain that offsets exactly the external dissipation of the coupled resonance.

The solid and dashed lines in Figs. 2(a) and 2(b) show the real (ω) and imaginary (γ) parts of the eigenvalues [see Eq. (7)] as a function of the detuning δ. For comparison, we numerically solve the eigenvalues of Eq. (5) at $G = 0.01\Gamma$ and $\tilde{U} = 10^{-3}\Gamma$ [see the circles and squares in Figs. 2(a) and 2(b)]. We see that the numerical and analytical results highly agree at a weak two-photon driving amplitude G. This validates the approximations we made in the calculations. Figure 2(b) shows that the spectrum of the dissipatively coupled system acquires a CIS in the limit $\delta = 0$ and $\gamma_0 \to 0$. The extreme condition $\gamma_0 = 0$ holds when none of the cavity modes suffers spontaneous losses from the surroundings while interacting with the mediating bath. The CIS has prodigious sensing potential, allowing efficient detection of nonlinearities in the configuration [31]. The physical origin of this peculiar behavior comes from an effective coupling induced between two modes in the presence of a shared reservoir.

The CIS was exploited to measure the response (mean excitation number for the system in steady state) of the system to the parameter change of the Kerr nonlinearity with only a single-photon drive in Ref. [31]. Here, we elaborate a different detection strategy through homodyne detection. Specifically, we perform a homodyne measurement on the cavity field $\tilde{b}$ to detect the weak nonlinearities with higher sensitivity. The key measurement quantity, in this case, is the amplitude and

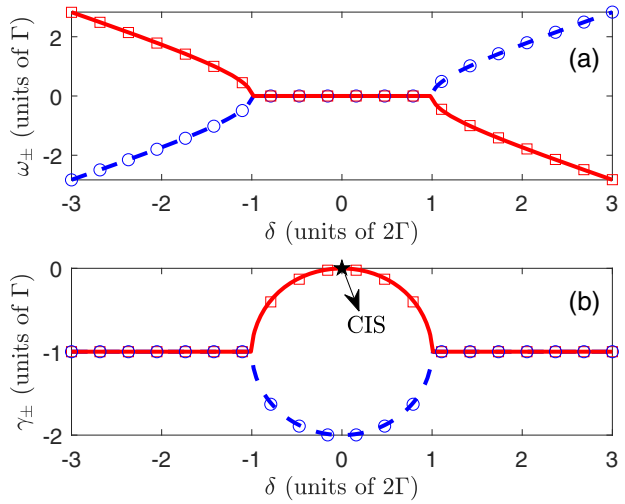

FIG. 2. (a) The real and (b) imaginary parts of the eigenvalues vs the detuning δ with $\gamma_0 = 10^{-5}\Gamma$. The circles and squares are the numerical results with $G = 0.01\Gamma$ and $\tilde{U} = 10^{-3}\Gamma$, while the solid and dashed lines represent the analytical approximation given in Eq. (7). The CIS is marked by the star. We study only the eigenvalue corresponding to α and β.

phase quadratures of the cavity field. Solving the steady-state solutions of Eq. (4), we obtain

$$\begin{aligned} -i[\delta/2 - i\gamma]\alpha - \Gamma\beta &= 0, \\ -\Gamma\alpha - i[-\delta/2 - i\gamma]\beta - 2iU|\beta|^2\beta - 2iG\beta^* &= i\Omega, \\ i[\delta/2 + i\gamma]\alpha^* - \Gamma\beta^* &= 0, \\ -\Gamma\alpha^* + i[-\delta/2 + i\gamma]\beta^* + 2iU|\beta|^2\beta^* + 2iG\beta &= -i\Omega. \end{aligned} \tag{8}$$

Eliminating α and α^*, we get

$$\begin{aligned} \frac{\Gamma^2\beta}{i\delta/2+\gamma} + (i\delta/2 - \gamma)\beta - 2iU|\beta|^2\beta - 2iG\beta^* &= i\Omega, \\ \frac{\Gamma^2\beta^*}{-i\delta/2+\gamma} + (-i\delta/2 - \gamma)\beta^* + 2iU|\beta|^2\beta^* + 2iG\beta &= -i\Omega, \end{aligned} \tag{9}$$

where $\gamma = \gamma_0 + \Gamma$. Defining the amplitude $X_{\tilde{b}} = \frac{b+b^\dagger}{\sqrt{2}}$ and the phase $Y_{\tilde{b}} = \frac{-i(b-b^\dagger)}{\sqrt{2}}$, the expressions for the amplitude and phase quadratures of the cavity mode $\tilde{b}$ are given by

$$\begin{aligned} \langle X_{\tilde{b}}\rangle &= \frac{\sqrt{2}\Omega}{-\frac{\Theta^2\gamma^2}{(\gamma^2+(\delta/2)^2)^2\left(\frac{(\delta/2)\Gamma^2}{\gamma^2+(\delta/2)^2}-\delta/2+2U|\beta|^2-2G\right)} - \left(\frac{(\delta/2)\Gamma^2}{\gamma^2+(\delta/2)^2} - \delta/2 + 2U|\beta|^2 + 2G\right)}, \\ \langle Y_{\tilde{b}}\rangle &= \frac{\sqrt{2}\Omega}{\frac{\Theta\gamma}{\gamma^2+(\delta/2)^2} + \frac{\gamma^2+(\delta/2)^2}{\Theta\gamma}\left[\left(\frac{(\delta/2)\Gamma^2}{\gamma^2+(\delta/2)^2} - \delta/2 + 2U|\beta|^2 + 2G\right)\left(\frac{(\delta/2)\Gamma^2}{\gamma^2+(\delta/2)^2} - \delta/2 + 2U|\beta|^2 - 2G\right)\right]}, \end{aligned} \tag{10}$$

where $\Theta = \Gamma^2 - \gamma^2 - (\delta/2)^2$. Especially, Θ becomes extremely small around the CIS, which will cause $\langle Y_{\tilde{b}}\rangle$ to converge to zero. However, the expression of the amplitude quadrature of the cavity field $\tilde{b}$ around the CIS can be further simplified as

$$|\langle X_{\tilde{b}}\rangle| \approx \frac{\Omega}{\sqrt{2}(U|\beta|^2 + G)}. \tag{11}$$

The introduction of the two-photon drive reduces the sensitivity of the sensor; nevertheless, we can eliminate this influence by setting $G \ll \tilde{U}$. In this situation, we can approximately obtain

$$|\langle X_{\tilde{b}}\rangle| \approx \frac{\Omega}{\sqrt{2}U|\beta|^2}. \tag{12}$$

Clearly, Eq. (12) shows an excellent nonlinear dependence of the amplitude $|\langle X_{\tilde{b}}\rangle|$ on the Kerr nonlinear coefficient U around the CIS. To validate the superiority of utilizing the CIS, we numerically plot the amplitude and phase averages of the cavity field $\tilde{b}$ as a function of the detuning δ in Figs. 3(a) and 3(b). In the absence of two-photon drive, the amplitude average $|\langle X_{\tilde{b}}\rangle|$ displays a sharp peak to U around the CIS. A similar result was obtained by homodyning the amplitude of the cavity field $\tilde{a}$. This suggests that the CIS is a useful tool for sensing the Kerr nonlinearity. In contrast to the amplitude average, the phase average has a dip near the CIS, as predicted by the second line of Eq. (10). To this extent, we can choose to measure the amplitude quadrature to estimate the Kerr nonlinear coefficient U. The corresponding sensitivity quantitatively characterizes the performance of the sensor operating at CIS. The sensitivity can be defined as

$$S = \left|\frac{d\langle X_{\tilde{b}}\rangle}{dU}\right| = \xi U^{-2}, \tag{13}$$

where $\xi = \Omega/(\sqrt{2}|\beta|^2)$. In order to reveal the advantages of our sensing mechanism, a comparison with a previous sensing protocol is necessary. For the previous nonlinearity sensor, the sensitivity was expressed as $S_0 = \zeta U^{-5/3}$ [31]. Figure 3(c) shows the normalized sensitivities S and S_0 versus U. The sensitivity of the proposed sensor has been considerably enhanced in comparison with the previous nonlinearity sensor. In addition, we note that the tuning of the phase θ_p of the two-photon drive plays an important role in enhancing the response of the system to Kerr nonlinearity. When we set $\theta_p = \pi$, Eq. (11) becomes

$$|\langle X_{\tilde{b}}\rangle| \approx \left|\frac{\Omega}{\sqrt{2}(U|\beta|^2 - G)}\right|, \tag{14}$$

where the sign of the two-photon driving amplitude G is flipped. This means that the response of the system to Kerr nonlinearity can be enhanced to some extent by increasing the

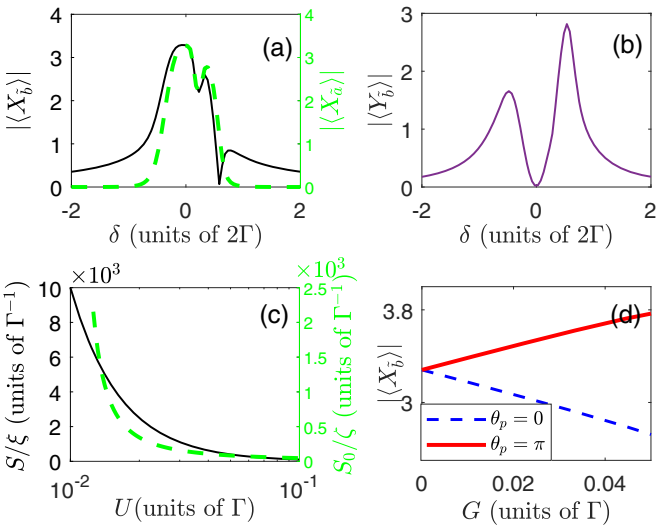

FIG. 3. (a) Average of the amplitude quadratures $|\langle X_{\tilde{b}}\rangle|$ (black) and $|\langle X_{\tilde{a}}\rangle|$ (bright green) for the system in steady state vs the detuning δ at $U = 0.02\Gamma$ and $G = 0$. (b) $|\langle Y_{\tilde{b}}\rangle|$ vs δ at $U = 0.02\Gamma$ and $G = 0$. (c) Contrast between the normalized sensitivities S/ξ (black) and S_0/ζ (bright green) when U is below 0.1Γ at $G = 0$. Notice that the coordinate scales for S and S_0 are different. (d) $|\langle X_{\tilde{b}}\rangle|$ vs G around the CIS at $U = 0.02\Gamma$. The other system parameters are the same as in Fig. 2.

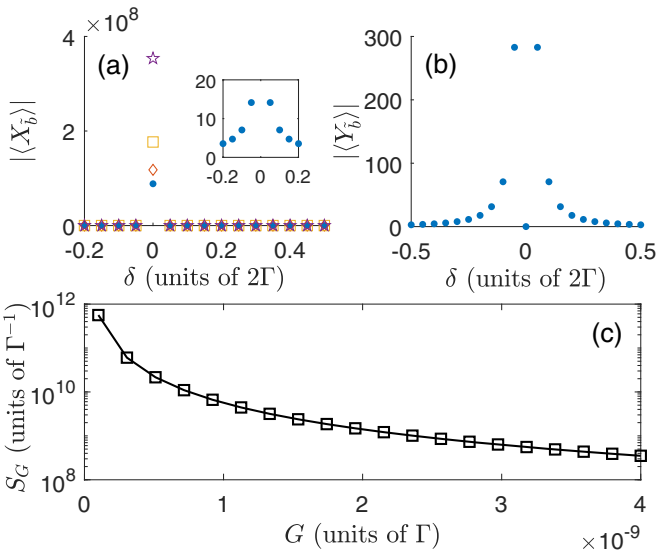

FIG. 4. (a) Average of the amplitude quadrature $|\langle X_{\tilde{b}}\rangle|$ for the system in steady state vs the detuning δ at four different strengths of the two-photon drive. The purple stars, yellow squares, orange diamonds, and blue solid circles correspond to $G = 1 \times 10^{-9}\Gamma$, $G = 2 \times 10^{-9}\Gamma$, $G = 3 \times 10^{-9}\Gamma$, and $G = 4 \times 10^{-9}\Gamma$, respectively. A significant response of the system to two-photon drive can be found around the CIS; otherwise, the response of the system to two-photon drive was weak (see the inset). (b) Average of the phase quadrature $|\langle Y_{\tilde{b}}\rangle|$ for the system in steady state vs the detuning δ at $G = 4 \times 10^{-9}\Gamma$. (c) The sensitivity S_G vs G around the CIS. The other system parameters are the same as in Fig. 2.

two-photon driving amplitude G. This analysis is in agreement with our numerical results in Fig. 3(d).

Another important finding of our work is that the system is also highly sensitive to the two-photon drive. We consider the case where the Kerr nonlinearity is weak with respect to the two-photon drive, at which point the Kerr nonlinearity can be safely ignored. In Figs. 4(a) and 4(b), we plot the amplitude and phase averages of the cavity field $\tilde{b}$ as a function of the detuning δ at four different strengths of the two-photon drive. Similarly, the amplitude average shows a striking response to U around the CIS. A weaker nonlinearity begets a higher response, as manifested in Fig. 4(a). And the phase average tends to zero around the CIS [see Fig. 4(b)]. In this case, the sensitivity of the system to the two-photon drive is obtained as follows:

$$S_G = \left|\frac{d\langle X_{\tilde{b}}\rangle}{dG}\right| \propto G^{-2}. \tag{15}$$

Clearly, near the CIS, the amplitude average becomes extremely sensitive to variations in G [see Fig. 4(c)], proving the efficiency of the CIS-based sensor in detecting the two-photon drive. Thus, our work provides a different way of estimating the two-photon driving amplitude for the CIS-based sensor.

B. The effect of fabrication imperfections on the sensitivity

The present scheme works for zero cavity-cavity couplings and ignorable intrinsic dampings. In realistic scenarios, however, fabrication imperfections are unavoidable. In this section, we investigate the effects of fabrication imperfections on the performance of the scheme. First, for a system consisting of two cavities with nonzero coupling J ($J \ll \Gamma$), the eigenvalues of Eq. (7) become $\tilde{\lambda}_\pm = -i\Gamma \pm \sqrt{(J - i\Gamma)^2 + \delta^2/4}$ at $\gamma_0 = 0$. We get a near-CIS around $\delta = 0$. Note that the amplitude and phase quadratures of Eq. (10) are now modified by replacing Γ^2 with $-(J - i\Gamma)^2$. We plot the modified response (amplitude average) of the system to the two-photon drive as a function of the direct coupling J around the CIS [see Fig. 5(a)]. The introduction of the direct coupling J between the two modes results in a decrease in the amplitude average, disrupting the performance of the CIS-based sensor. Second, the nonzero γ_0 (with a finite linewidth) also results in a decrease in the response [see Fig. 5(b)], and this decrease can be canceled by appropriately increasing the single-photon driving amplitude Ω [see Fig. 5(c)]. A single-photon driving amplitude close to 2.61Γ returns an amplitude average corresponding to zero intrinsic damping. Similar conclusions can be obtained for the sensing of Kerr nonlinearity. In contrast to the sensing of the two-photon drive, we need to increase the two-photon driving amplitude only slightly to overcome the deleterious effects of fabrication imperfections, as revealed in Fig. 5(d). In this sense, the present work provides a different method for a CIS-based sensor that is robust against defects or fabrication imperfections.

IV. DISCUSSION OF EXPERIMENTAL FEASIBILITY

Owing to recent progress in nanofabrication, our sensing protocol can be realized in experiments [68,69]. Here, we consider a silicon integrated photonic apparatus comprising

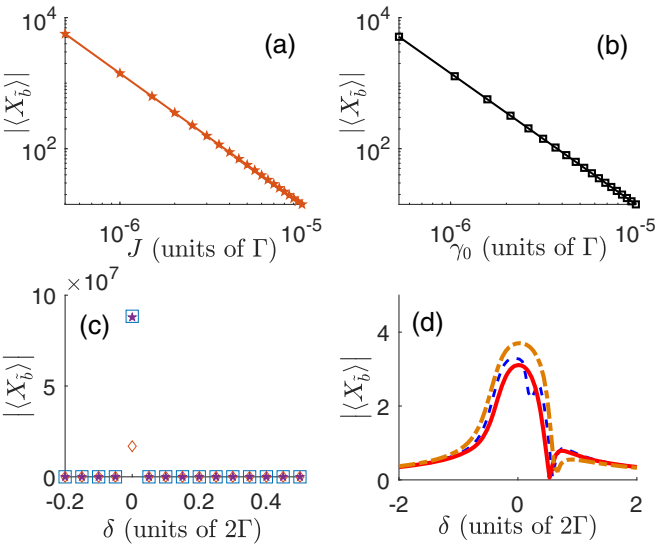

FIG. 5. (a) The response of the system to two-photon drive as a function of the direct coupling J around the CIS at $\gamma_0 = 0$, $G = 4 \times 10^{-9}\Gamma$, and $\Omega = 0.5\Gamma$. (b) The response of the system to two-photon drive vs the intrinsic damping γ_0 around the CIS at $G = 4 \times 10^{-9}\Gamma$ and $\Omega = 0.5\Gamma$. (c) The response of the system to two-photon drive vs the detuning δ at $G = 4 \times 10^{-9}\Gamma$. The blue squares indicate the response at $\gamma_0 = 0$ and $\Omega = 0.5\Gamma$, the orange diamonds show the response at $\gamma_0 = 10^{-8}\Gamma$ and $\Omega = 0.5\Gamma$, and the purple solid stars represent the response at $\gamma_0 = 10^{-8}\Gamma$ and $\Omega = 2.61\Gamma$. (d) The response of the system to Kerr nonlinearity as a function of the detuning δ at $\theta_p = \pi$, $\Omega = 0.5\Gamma$, and $U = 0.02\Gamma$. The blue dashed line shows the response at $\gamma_0 = 10^{-5}\Gamma$ and $G = 0$, the red solid line denotes the response at $\gamma_0 = 0.03\Gamma$ and $G = 0$, and the orange dash-dotted line indicates the response at $\gamma_0 = 0.03\Gamma$ and $G = 0.05\Gamma$.

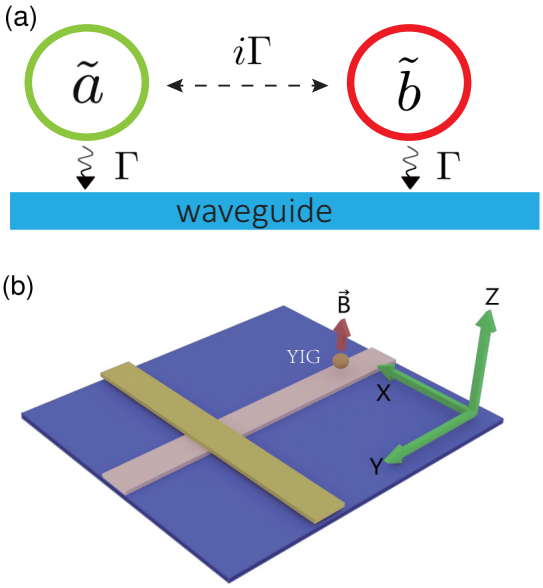

FIG. 6. (a) Schematic of the dual-resonator system that demonstrates the CIS. The two microring resonators are dissipatively coupled through a 1D waveguide. The effective dissipative coupling strength between the two modes is $i\Gamma$. (b) Schematic of the cavity-magnonic setup. The device consists of a yttrium iron garnet (YIG) sphere and a cross-line microwave circuit. An external magnetic field $\vec{B}$ aligned along the Z axis produces the Kittel mode in YIG.

two microring resonators; both of them are coupled to a one-dimensional (1D) waveguide, as depicted in Fig. 6(a). The two microring resonators have a radius of 3.1 μm and a waveguide width of 0.4 μm. The gaps between the microring resonators and the waveguide are 0.1 μm. In the setup, the silicon has a negligible intrinsic damping in the communication band (∼1550 nm). The resonant frequency can be tuned precisely by the electro-optic effects. Owing to the large distance between the two resonators, the direct coupling between them can be ignored. Thus, such a configuration constitutes a good benchmark to test our protocol.

To make our protocol work, a driving laser of frequency ω_l is applied to mode $\tilde{b}$; the field amplitudes are given by $\Omega = \sqrt{\kappa_j P_l/\hbar\omega_l}$ ($j = \tilde{a}, \tilde{b}$), where P_l is the input laser power. A two-photon drive can be realized via optical parametric down-conversion. Within the reach of current experiment [68], the system parameters in this study can be chosen to be $\Gamma = 1334$ GHz and $Q \sim 10^4$ (Q factor). Using these together with the attainable two-photon driving amplitude $G \in [133.4, 5336]$ Hz, the response of the system to two-photon drive falls in the region of $(3.536–0.088) \times 10^9$.

We would like to mention that our protocol is not limited to this particular architecture. For example, it can be realized in the cavity-magnon configurations reported in [70–76]. Here, we consider a setup that consists of a microwave cavity and a yttrium iron garnet (YIG) sphere, both interfacing with a 1D waveguide [see Fig. 6(b)]. The microwave cavity is subject to a two-photon drive of amplitude G and a microwave field with the Rabi frequency Ω. Due to the absence of spatial overlap between the optical cavity and magnon modes, the direct coupling between them can be safely ignored. The interaction with the waveguide induces a dissipative magnon-photon coupling with $\Gamma = 2\pi \times 10$ MHz. With an achievable two-photon driving amplitude range $G \in [0.0063, 0.2513]$ Hz, our sensing protocol theoretically predicts that the response of the system to the two-photon drive falls in the range of $(3.536–0.088) \times 10^9$. It can also be seen that the response of the system to two-photon drive is greatly increased for weak two-photon driving amplitude. This validates the efficiency of the CIS-based sensor in detecting weak nonlinearities.

V. CONCLUSION

In conclusion, we have proposed a mechanism to enhance the sensitivity of the system to nonlinearities by homodyning the amplitude quadrature of the cavity field. The system consists of two dissipatively coupled cavity modes, one of which is subject to single- and two-photon drives. For low two-photon driving strength, the spectrum of the dissipatively coupled system acquires a CIS, which exhibits high sensitivity to weak nonlinearities. The physical origin of this peculiar behavior lies in the effective coupling induced between two modes in the presence of a common reservoir. Compared to the previous sensing protocol, the sensor achieves an unprecedented sensitivity around the CIS. We illustrated the sensing capabilities in two scenarios, one with a silicon integrated photonic apparatus and the other with a cavity-magnonic

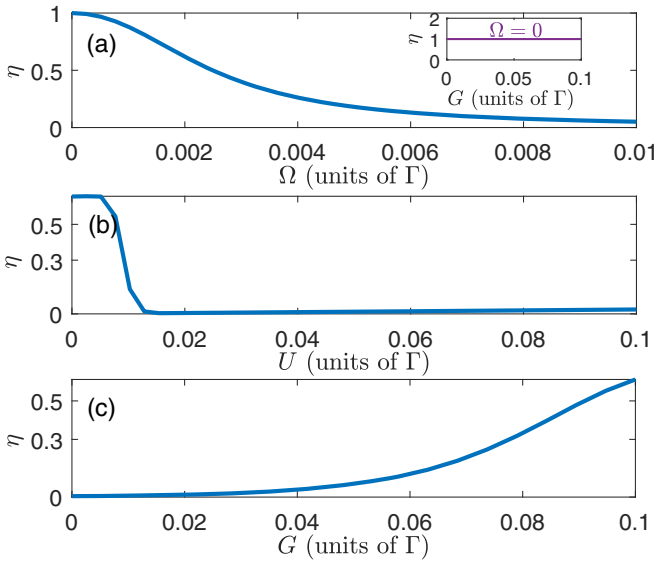

FIG. 7. (a) The relative error η due to the mean-field approximation vs the amplitude Ω of the single-photon drive at $G = 10^{-3}\Gamma$ and $U = 10^{-3}\Gamma$. Inset: η vs G at $\Omega = 0$ and $U = 10^{-3}\Gamma$. (b) The relative error η due to the mean-field approximation vs the Kerr nonlinearity coefficient U at $G = 0$ and $\Omega = 0.5\Gamma$. (c) η vs G at $U = 0.02\Gamma$ and $\Omega = 0.5\Gamma$. The other parameters chosen are $\delta = 0$ and $\gamma_0 = 10^{-5}\Gamma$.

setup. Our scheme is robust against the fluctuations and opens a different avenue for weak nonlinearities. It is worth noting that our scheme does not require anti-$\mathcal{PT}$ symmetry and can be extended to a plethora of systems, including, laser-cooled atomic ensembles [30], superconducting transmon qubits [77], and optomechanical systems [78–81]. Although we focus here on estimating a nonlinear parameter, our sensing protocol, in principle, can also be applied to estimate the linear parameter.

ACKNOWLEDGMENTS

This work is supported by the National Natural Science Foundation of China (NSFC) under Grants No. 12175033 and No. 12147206 and the National Key R&D Program of China under Grant No. 2021YFE0193500.

APPENDIX: THE VALIDITY OF THE MEAN-FIELD APPROXIMATION

In this Appendix, we discuss the validity of the mean-field approximation. First, we numerically plot the relative error due to the mean-field approximation defined by $\eta = \frac{|\langle b^\dagger bb\rangle - \langle b^\dagger\rangle\langle b\rangle\langle b\rangle|}{|\langle b^\dagger bb\rangle|}$ versus the amplitude Ω of the single-photon drive [see Fig. 7(a)]. It can be seen that when the system is in the steady state, the relative error η due to the mean-field approximation can reach 100% before the introduction of the single-photon drive (i.e., $\Omega = 0$). By further increasing the two-photon driving amplitude G, η remains unchanged (see the inset). With the introduction of the single-photon drive, the relative error η decreases gradually and is less than 30% in the region that interests us. Moreover, we numerically plot the relative error η due to the mean-field approximation as a function of U at $G = 0$ and $\Omega = 0.5\Gamma$ and show the results in Fig. 7(b). We can find that when the system is in the steady state, the relative error is less than 30% for parameter region $U \in [0.01, 0.1]\Gamma$. In the presence of the two-photon drive, this mean-field approximation remains valid in the parameter interval $G \in [0, 0.079]\Gamma$ for a fixed Kerr nonlinearity coefficient $U = 0.02\Gamma$ [see Fig. 7(c)].

[1] C. M. Bender and S. Boettcher, Real Spectra in Non-Hermitian Hamiltonians Having $\mathcal{PT}$ Symmetry, Phys. Rev. Lett. **80**, 5243 (1998).
[2] C. M. Bender, D. C. Brody, and H. F. Jones, Complex Extension of Quantum Mechanics, Phys. Rev. Lett. **89**, 270401 (2002).
[3] C. M. Bender, Making sense of non-Hermitian Hamiltonians, Rep. Prog. Phys. **70**, 947 (2007).
[4] M. V. Berry, Physics of nonhermitian degeneracies, Czech. J. Phys. **54**, 1039 (2004).
[5] W. D. Heiss, The physics of exceptional points, J. Phys. A **45**, 444016 (2012).
[6] R. El-Ganainy, K. G. Makris, D. N. Christodoulides, and Z. H. Musslimani, Theory of coupled optical PT-symmetric structures, Opt. Lett. **32**, 2632 (2007).
[7] A. Guo, G. J. Salamo, D. Duchesne, R. Morandotti, M. Volatier-Ravat, V. Aimez, G. A. Siviloglou, and D. N. Christodoulides, Observation of $\mathcal{PT}$-Symmetry Breaking in Complex Optical Potentials, Phys. Rev. Lett. **103**, 093902 (2009).
[8] C. E. Rüter, K. G. Makris, R. El-Ganainy, D. N. Christodoulides, M. Segev, and D. Kip, Observation of parity-time symmetry in optics, Nat. Phys. **6**, 192 (2010).
[9] B. Peng, Ş. K. Özdemir, F. Lei, F. Monifi, M. Gian-freda, G. L. Long, S. Fan, F. Nori, C. M. Bender, and L. Yang, Parity-time-symmetric whispering-gallery microcavities, Nat. Phys. **10**, 394 (2014).
[10] C. Hang, G. Huang, and V. V. Konotop, $\mathcal{PT}$ Symmetry with a System of Three-Level Atoms, Phys. Rev. Lett. **110**, 083604 (2013).
[11] Z. Zhang, Y. Zhang, J. Sheng, L. Yang, M.-A. Miri, D. N. Christodoulides, B. He, Y. Zhang, and M. Xiao, Observation of Parity-Time Symmetry in Optically Induced Atomic Lattices, Phys. Rev. Lett. **117**, 123601 (2016).
[12] R. Fleury, D. Sounas, and A. Alù, An invisible acoustic sensor based on parity-time symmetry, Nat. Commun. **6**, 5905 (2015).
[13] X.-W. Xu, Y.-X. Liu, C.-P. Sun, and Y . Li, Mechanical $\mathcal{PT}$ symmetry in coupled optomechanical systems, Phys. Rev. A **92**, 013852 (2015).
[14] X. Zhu, H. Ramezani, C. Shi, J. Zhu, and X. Zhang, $\mathcal{PT}$-Symmetric Acoustics, Phys. Rev. X **4**, 031042 (2014).
[15] L. Feng, Z. J. Wong, R.-M. Ma, Y. Wang, and X. Zhang, Single-mode laser by parity-time symmetry breaking, Science **346**, 972 (2014).
[16] H. Hodaei, M.-A. Miri, M. Heinrich, D. N. Christodoulides, and M. Khajavikhan, Parity-time-symmetric microring lasers, Science **346**, 975 (2014).

[17] J. Wiersig, Enhancing the Sensitivity of Frequency and Energy Splitting Detection by Using Exceptional Points: Application to Microcavity Sensors for Single-Particle Detection, Phys. Rev. Lett. **112**, 203901 (2014).

[18] Z.-P. Liu, J. Zhang, Ş. K. Özdemir, B. Peng, H. Jing, X.-Y. Lü, C.-W. Li, L. Yang, F. Nori, and Y.-X. Liu, Metrology with $\mathcal{PT}$-Symmetric Cavities: Enhanced Sensitivity near the $\mathcal{PT}$-Phase Transition, Phys. Rev. Lett. **117**, 110802 (2016).

[19] R. El-Ganainy, K. G. Makris, M. Khajavikhan, Z. H. Musslimani, S. Rotter, and D. N. Christodoulides, Non-Hermitian physics and PT symmetry, Nat. Phys. **14**, 11 (2018).

[20] W. Chen, Ş. K. Özdemir, G. Zhao, J. Wiersig and L. Yang, Exceptional points enhance sensing in an optical microcavity, Nature (London) **548**, 192 (2017).

[21] H. Hodaei, A. U. Hassan, S. Wittek, H. Garcia-Gracia, R. El-Ganainy, D. N. Christodoulides, and M. Khajavikhan, Enhanced sensitivity at higher-order exceptional points, Nature (London) **548**, 187 (2017).

[22] J. Doppler, A. A. Mailybaev, J. Böhm, U. Kuhl, A. Girschik, F. Libisch, T. J. Milburn, P. Rabl, N. Moiseyev, and S. Rotter, Dynamically encircling an exceptional point for asymmetric mode switching, Nature (London) **537**, 76 (2016).

[23] Q. Wang, J. Wang, H. Z. Shen, S. C. Hou, and X. X. Yi, Exceptional points and dynamics of a non-Hermitian two-level system without PT symmetry, Europhys. Lett. **131**, 34001 (2020).

[24] H. Xu, D. Mason, L. Jiang, and J. G. E. Harris, Topological energy transfer in an optomechanical system with exceptional points, Nature (London) **537**, 80 (2016).

[25] H. Jing, S. K. Özdemir, X.-Y. Lü, J. Zhang, L. Yang, and F. Nori, $\mathcal{PT}$-Symmetric Phonon Laser, Phys. Rev. Lett. **113**, 053604 (2014).

[26] J. Schindler, A. Li, M. C. Zheng, F. M. Ellis, and T. Kottos, Experimental study of active LRC circuits with $\mathcal{PT}$ symmetries, Phys. Rev. A **84**, 040101(R) (2011).

[27] J. Rubinstein, P. Sternberg, and Q. Ma, Bifurcation Diagram and Pattern Formation of Phase Slip Centers in Superconducting Wires Driven with Electric Currents, Phys. Rev. Lett. **99**, 167003 (2007).

[28] S. Bittner, B. Dietz, U. Günther, H. L. Harney, M. Miski-Oglu, A. Richter, and F. Schäfer, PT Symmetry and Spontaneous Symmetry Breaking in a Microwave Billiard, Phys. Rev. Lett. **108**, 024101 (2012).

[29] L. Feng, M. Ayache, J. Huang, Y.-L. Xu, M.-H. Lu, Y.-F. Chen, Y. Fainman, and A. Scherer, Nonreciprocal light propagation in a silicon photonic circuit, Science **333**, 729 (2011).

[30] Y. Jiang, Y. Mei, Y. Zuo, Y. Zhai, J. Li, J. Wen, and S. Du, Anti-Parity-Time Symmetric Optical Four-Wave Mixing in Cold Atoms, Phys. Rev. Lett. **123**, 193604 (2019).

[31] J. M. P. Nair, D. Mukhopadhyay, and G. S. Agarwal, Enhanced Sensing of Weak Anharmonicities through Coherences in Dissipatively Coupled Anti-PT Symmetric Systems, Phys. Rev. Lett. **126**, 180401 (2021).

[32] L. Ge and H. E. Türeci, Antisymmetric $\mathcal{PT}$-photonic structures with balanced positive- and negative-index materials, Phys. Rev. A **88**, 053810 (2013).

[33] P. Peng, W. Cao, C. Shen, W. Qu, J. Wen, L. Jiang, and Y. Xiao, Anti-parity-time symmetry with flying atoms, Nat. Phys. **12**, 1139 (2016).

[34] V. V. Konotop and D. A. Zezyulin, Odd-Time Reversal $\mathcal{PT}$ Symmetry Induced by an Anti-$\mathcal{PT}$-Symmetric Medium, Phys. Rev. Lett. **120**, 123902 (2018).

[35] X.-L. Zhang, S. Wang, B. Hou, and C. T. Chan, Dynamically Encircling Exceptional Points: In Situ Control of Encircling Loops and the Role of the Starting Point, Phys. Rev. X **8**, 021066 (2018).

[36] Y. Li, Y.-G. Peng, L. Han, M.-A. Miri, W. Li, M. Xiao, X.-F. Zhu, J. Zhao, A. Alù, S. Fan, and C.-W. Qiu, Anti-parity-time symmetry in diffusive systems, Science **364**, 170 (2019).

[37] Y.-L. Chuang, Ziauddin, and R. K. Lee, Realization of simultaneously parity-time-symmetric and parity-time-antisymmetric susceptibilities along the longitudinal direction in atomic systems with all optical controls, Opt. Express **26**, 21969 (2018).

[38] D. A. Antonosyan, A. S. Solntsev, and A. A. Sukhorukov, Parity-time anti-symmetric parametric amplifier, Opt. Lett. **40**, 4575 (2015).

[39] J. Zhao, Y. Liu, L. Wu, C.-K. Duan, Y.-X. Liu, and J. Du, Observation of Anti-$\mathcal{PT}$-Symmetry Phase Transition in the Magnon-Cavity-Magnon Coupled System, Phys. Rev. Appl. **13**, 014053 (2020).

[40] Y. Choi, C. Hahn, J. W. Yoon, and S. H. Song, Observation of an anti-PT-symmetric exceptional point and energy-difference conserving dynamics in electrical circuit resonators, Nat. Commun. **9**, 2182 (2018).

[41] F. Yang, Y.-C. Liu, and L. You, Anti-$\mathcal{PT}$ symmetry in dissipatively coupled optical systems, Phys. Rev. A **96**, 053845 (2017).

[42] H. Fan, J. Chen, Z. Zhao, J. Wen, and Y.-P. Huang, Antiparity-time symmetry in passive nanophotonics, ACS Photonics **7**, 3035 (2020).

[43] Q. Li, C. J. Zhang, Z. D. Cheng, W. Z. Liu, J. F. Wang, F. F. Yan, Z. H. Lin, Y. Xiao, K. Sun, Y. T. Wang, J. S. Tang, J. S. Xu, C. F. Li, and G. C. Guo, Experimental simulation of anti-parity-time symmetric Lorentz dynamics, Optica **6**, 67 (2019).

[44] I. I. Arkhipov and F. Minganti, Emergent non-Hermitian localization phenomena in the synthetic space of zero-dimensional bosonic systems, Phys. Rev. A **107**, 012202 (2023).

[45] H. Zhang, R. Huang, S.-D. Zhang,Y . Li, C.-W. Qiu, F. Nori, and H. Jing, Breaking anti-PT symmetry by spinning a resonator, Nano Lett. **20**, 7594 (2020).

[46] J. Wiersig, Prospects and fundamental limits in exceptional point-based sensing, Nat. Commun. **11**, 2454 (2020).

[47] S. Scheel and A. Szameit, $\mathcal{PT}$-symmetric photonic quantum systems with gain and loss do not exist, Europhys. Lett. **122**, 34001 (2018).

[48] M.-A. Miri and A. Alu, Exceptional points in optics and photonics, Science **363**, eaar7709 (2019).

[49] Ş. K. Özdemir, S. Rotter, F. Nori, and L. Yang, Parity-time symmetry and exceptional points in photonics, Nat. Mater. **18**, 783 (2019).

[50] P. Djorwe, Y. Pennec, and B. Djafari-Rouhani, Frequency locking and controllable chaos through exceptional points in optomechanics, Phys. Rev. E **98**, 032201 (2018).

[51] P. Djorwe, Y. Pennec, and B. Djafari-Rouhani, Exceptional Point Enhances Sensitivity of Optomechanical Mass Sensors, Phys. Rev. Appl. **12**, 024002 (2019).

[52] T. Li, W. Wang, and X. X. Yi, Enhancing the sensitivity of optomechanical mass sensors with a laser in a squeezed state, Phys. Rev. A **104**, 013521 (2021).

[53] D. Cui, T. Li, J. N. Li, and X. X. Yi, Detecting deformed commutators with exceptional points in optomechanical sensors, New J. Phys. **23**, 123037 (2021).

[54] X. Mao, G.-Q. Qin, H. Yang, H. Zhang, M. Wang, and G.-L. Long, Enhanced sensitivity of optical gyroscope in a mechanical parity-time-symmetric system based on exceptional point, New J. Phys. **22**, 093009 (2020).

[55] M. J. Grant and M. J. Digonnet, Rotation sensitivity and shot-noise-limited detection in an exceptional-point coupled-ring gyroscope, Opt. Lett. **46**, 2936 (2021).

[56] G. S. Agarwal, *Quantum Optics* (Springer, New York, 1974).

[57] M. Aspelmeyer, T. J. Kippenberg, and F. Marquardt, Cavity optomechanics, Rev. Mod. Phys. **86**, 1391 (2014).

[58] D. K. Bayen and S. Mandal, Classical and quantum description of a periodically driven multi-photon anharmonic oscillator, Opt. Quantum Electron. **51**, 388 (2019).

[59] D. K. Bayen and S. Mandal, Squeezing of coherent light coupled to a periodically driven two-photon anharmonic oscillator, Eur. Phys. J. Plus **135**, 408 (2020).

[60] D. K. Bayen and S. Mandal, Quantum dynamics and frequency shift of a periodically driven multi-photon anharmonic oscillator, in *Quantum Collisions and Confinement of Atomic and Molecular Species, and Photons: Select Proceedings of the 7th Topical Conference of ISAMP 2018*, edited by P. C. Deshmukh, E. Krishnakumar, S. Fritsche, M. Krishnamurthy, and S. Majumder (Springer, Singapore, 2019), pp. 100–105.

[61] C. C. Gerry, Squeezing from k-photon anharmonic oscillators, Phys. Lett. A **124**, 237 (1987).

[62] V. Bužek, Periodic revivals of squeezing in an anharmonic-oscillator model with coherent light, Phys. Lett. A **136**, 188 (1989).

[63] R. Tanas, Squeezing from an anharmonic oscillator model: $(a^\dagger)^2a^2$ versus $(a^\dagger a)^2$ interaction Hamiltonians, Phys. Lett. A **141**, 217 (1989).

[64] C. Gerry and P. Knight, *Introductory Quantum Optics* (Cambridge University Press, Cambridge, 2005).

[65] R. W. Boyd, *Nonlinear Optics* (Academic, New York, 2008).

[66] Z. Leghtas, S. Touzard, I. M. Pop, A. Kou, B. Vlastakis, A. Petrenko, K. M. Sliwa, A. Narla, S. Shankar, M. J. Hatridge, M. Reagor, L. Frunzio, R. J. Schoelkopf, M. Mirrahimi, and M. H. Devoret, Confining the state of light to a quantum manifold by engineered two-photon loss, Science **347**, 853 (2015).

[67] A. Metelmann and A. A. Clerk, Nonreciprocal Photon Transmission and Amplification via Reservoir Engineering, Phys. Rev. X **5**, 021025 (2015).

[68] Z. Gong, J. Serafini, F. Yang, S. Preble, and J. Yao, Bound States in the Continuum on a Silicon Chip with Dynamic Tuning, Phys. Rev. Appl. **16**, 024059 (2021).

[69] J. Zhang, Z. Feng, and X. Sun, Realization of bound states in the continuum in anti-*PT*-symmetric optical systems: A proposal and analysis, Laser Photonics Rev. 2200079 (2022).

[70] J. M. P. Nair and G. S. Agarwal, Deterministic quantum entanglement between macroscopic ferrite samples, Appl. Phys. Lett. **117**, 084001 (2020).

[71] Y. Zhou, J. Xu, S. Xie, and Y. Yang, Squeezed driving induced entanglement and squeezing among cavity modes and magnon mode in a magnon-cavity QED system, arXiv:2201.09154.

[72] Y.-P. Wang, J. W. Rao, Y. Yang, P.-C. Xu, Y. S. Gui, B. M. Yao, J. Q. You, and C.-M. Hu, Nonreciprocity and Unidirectional Invisibility in Cavity Magnonics, Phys. Rev. Lett. **123**, 127202 (2019).

[73] Y. Yang, Y.-P. Wang, J. W. Rao, Y. S. Gui, B. M. Yao, W. Lu, and C.-M. Hu, Unconventional Singularity in Anti-Parity-Time Symmetric Cavity Magnonics, Phys. Rev. Lett. **125**, 147202 (2020).

[74] M. Harder, Y. Yang, B. M. Yao, C. H. Yu, J. W. Rao, Y. S. Gui, R. L. Stamps, and C.-M. Hu, Level Attraction Due to Dissipative Magnon-Photon Coupling, Phys. Rev. Lett. **121**, 137203 (2018).

[75] Y.-P. Wang, G.-Q. Zhang, D. Zhang, X.-Q. Luo, W. Xiong, S.-P. Wang, T.-F. Li, C.-M. Hu, and J. Q. You, Magnon Kerr effect in a strongly coupled cavity-magnon system, Phys. Rev. B **94**, 224410 (2016).

[76] J. W. Rao, Y. P. Wang, Y. Yang, T. Yu, Y. S. Gui, X. L. Fan, D. S. Xue, and C.-M. Hu, Interactions between a magnon mode and a cavity photon mode mediated by traveling photons, Phys. Rev. B **101**, 064404 (2020).

[77] J. Koch, T. M. Yu, J. Gambetta, A. A. Houck, D. I. Schuster, J. Majer, A. Blais, M. H. Devoret, S. M. Girvin, and R. J. Schoelkopf, Charge-insensitive qubit design derived from the Cooper pair box, Phys. Rev. A **76**, 042319 (2007).

[78] N. R. Bernier, L. D. Tóth, A. K. Feofanov, and T. J. Kippenberg, Level attraction in a microwave optomechanical circuit, Phys. Rev. A **98**, 023841 (2018).

[79] Y. Yu, X. Xi, and X. Sun, Observation of bound states in the continuum in a micromechanical resonator, arXiv:2109.09498.

[80] Q. Zhang, C. Yang, J. Sheng, and H. Wu, Dissipative coupling induced phonon lasing with anti-parity-time symmetry, arXiv:2110.12456.

[81] K. Stannigel, P. Rabl, A. S. Sørensen, P. Zoller, and M. D. Lukin, Optomechanical Transducers for Long-Distance Quantum Communication, Phys. Rev. Lett. **105**, 220501 (2010).